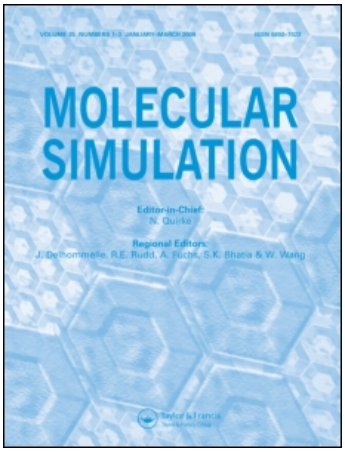

Molecular Simulation
Publication details, including instructions for authors and subscription information:
http://www.informaworld.com/smpp/title~content=t713644482

Quantum nature of adsorbed hydrogen on single-wall carbon nanohorns

H. Tanaka[a]; J. Fan[b]; H. Kanoh[c]; M. Yudasaka[bd]; S. Iijima[bde]; K. Kaneko[c]
[a] Diversity and Fractal Science, Graduate School of Science and Technology, Chiba University, Chiba, Japan [b] SORST, Japan Science and Technology Agency, Tsukuba, Japan [c] Department of Chemistry, Faculty of Science, Chiba University, Chiba, Japan [d] NEC Corporation, Tsukuba, Japan [e] Department of Physics, Meijo University, Nagoya, Japan

To cite this Article Tanaka, H. , Fan, J. , Kanoh, H. , Yudasaka, M. , Iijima, S. and Kaneko, K.(2005) 'Quantum nature of adsorbed hydrogen on single-wall carbon nanohorns', Molecular Simulation, 31: 6, 465 — 474
To link to this Article: DOI: 10.1080/08927020412331337032
URL: http://dx.doi.org/10.1080/08927020412331337032

Molecular Simulation, Vol. 31, Nos. 6–7, 15 May – 30 May 2005, 465–474

Quantum nature of adsorbed hydrogen on single-wall carbon nanohorns

H. TANAKA†, J. FAN‡, H. KANOH¶, M. YUDASAKA‡§, S. IIJIMA‡§‖ and K. KANEKO¶*

†Diversity and Fractal Science, Graduate School of Science and Technology, Chiba University, 1-33 Yayoi, Inage, Chiba 263-8522, Japan
‡SORST, Japan Science and Technology Agency, c/o NEC Corporation, 34 Miyukigaoka, Tsukuba 305-8501, Japan
¶Department of Chemistry, Faculty of Science, Chiba University, 1-33 Yayoi, Inage, Chiba 263-8522, Japan
§NEC Corporation, 34 Miyukigaoka, Tsukuba 305-8501, Japan
‖Department of Physics, Meijo University, 1-501 Shiogamaguchi, Tenpaku, Nagoya 468-8502, Japan

(Received November 2004; In final form December 2004)

We have measured N_2 adsorption isotherms on single-wall carbon nanohorns (SWNHs) over the temperature range of 77–92 K, and isosteric heat of adsorption, q_{st}, were determined. Adsorption measurements for SWNHs have been also done for for H_2 at 20 K, and for H_2 and D_2 at 77 K, respectively. We have performed grand canonical Monte Carlo (GCMC) simulations of N_2, H_2, and D_2 for single-wall carbon nanotube (SWNT) models to compare with the experimental data. Simulated N_2 adsorption isotherm on a SWNT bundle model is in reasonably good agreement with the experimental isotherm on the SWNH assembly over a wide range of pressures at 77 K; however, simulated q_{st}-values for the SWNT bundle suggest that the SWNH particles are incompletely arranged in the SWNH assembly. Simulated endohedral isotherm of classical H_2 inside an isolated SWNT model at 20 K showed that a density of adsorbed H_2 in the internal space of the SWNH particle is quite smaller than that of classical H_2 because of large quantum effects. In simulating H_2 and D_2 adsorption isotherms on the model SWNT bundle at 77 K, GCMC simulations based on the Feynman-Hibbs (FH) effective potential were applied to introduce quantum effects to the statistical properties generated by the classical Lennard-Jones (LJ) potential. We found that an adsorption ratio of H_2 to D_2 on the SWNT bundle from the FH-GCMC simulations is less than 0.91 depending on adsorption pressure; this is because the potential field of the SWNT bundle for H_2 is relatively weaker than that for D_2 even at 77 K, due to the wide quantum spreading of a H_2 molecule.

Keywords: Hydrogen; Adsorption; Nanohorn; Simulation; Quantum effects

1. Introduction

Discovery of single-wall carbon nanotube (SWNT) in 1993 [1,2] has brought a new research subject of hydrogen storage by SWNTs; experimental reports on great hydrogen capacity of SWNTs [3,4] were examined by many molecular simulation studies [5–7]. These simulation studies showed that the large H_2 storage capacities experimentally obtained for impure SWNT samples cannot be reproduced at ambient temperature. In their simulations, H_2 molecule was assumed to be a classical particle; however, Wang and Johnson suggested that quantum effects should be explicitly taken into account to understand the adsorption of H_2 on SWNTs and their interstitial channels over a wide range of temperatures using path-integral Monte Carlo (PIMC) technique [8]. In view of experiments, however, we do not yet have a reliable hydrogen adsorption data on SWNTs over the range of temperatures from 20 K (the normal boiling temperature of H_2) to ambient temperature. This is because H_2 adsorption measurements need sufficient amount of samples of high purity (more than 100 mg for static adsorption measurements). Consequently, we have not evidence yet the importance of quantum effects on H_2 adsorption on SWNTs experimentally. However, Setoyama and Kaneko reported an unusual behavior of He in slit-shaped graphitic nanopores of activated carbon fibers (ACFs) at 4.2 K [9]. Nemirovsky *et al.* showed quantum effects on the kinetic energy of adsorbed He and Ne in the carbon slit pores of ACFs at low temperatures [10,11]. We studied Ne adsorption on $AlPO_4$-5 at 27 K by comparing experimental adsorption isotherms with classical DFT calculations, showing a quantum contribution to the configuration of the adsorbed Ne atoms in the

*Corresponding author. Tel.: +81-43-290-2779, Fax: +81-43-290-2788. E-mail: kaneko@pchem2.s.chiba-u.ac.jp

Molecular Simulation
ISSN 0892-7022 print/ISSN 1029-0435 online © 2005 Taylor & Francis Group Ltd
http://www.tandf.co.uk/journals
DOI: 10.1080/08927020412331337032

quasi one-dimensional (1D) channel below 33 K [12]. Therefore, the study on quantum effects on physical adsorption is now one of the attractive subjects in the filed of adsorption.

Recently Iijima *et al.* prepared single-wall carbon nanohorn (SWNH) of which fundamental tube structure is similar to SWNTs [13]. SWNH can be produced by a CO_2 laser abrasion of pure graphite in Ar atmosphere without any metal catalysts at room temperature. SWNH has a typical tube diameter of about 3 nm with length in the range of 30–50 nm, and a conical cap at the end of the tube. The apex of the conical cap is about 20°. SWNHs are associated each other to form a *dahlia* flower-like assembly (diameter 80 ~ 100 nm), providing nanoporosity [14–17] (A TEM image of the SWNT assembly is shown in figure 1 with a schematic representation of the SWNH particles). Abundant SWNHs of several grams with high purity (>90%) can be easily produced. The preceding particle density measurement of SWNHs showed that the SWNH particles were completely closed, and the internal tube spaces were not available for gas adsorption. However, an oxidation of the SWNH sample in O_2 atmosphere at 693 K can produce nanoscale windows on the wall of the SWNH particle [16]. Therefore, a separative determination of adsorption in the internal tube and interstitial channels between SWNHs can be carried out in case of the SWNH assembly. In the previous work, we determined the adsorbed density of H_2 inside the SWNH particles at 20 K, indicating an explicit quantum contribution to the density of adsorbed H_2 [18].

In the present study, N_2 adsorption isotherms on SWNHs have been measured over the temperature range 77–92 K and isosteric heats of adsorption, q_{st}, were calculated. We compared the N_2 adsorption isotherm at 77 K and q_{st} with those from grand canonical Monte Carlo (GCMC) simulations [19] for a simplified SWNT bundle model. Adsorption isotherm of H_2 on SWNHs was also obtained at 20 K, and compared with the simulated isotherm of classical H_2 inside an isolated SWNT model. In simulating H_2 and D_2 adsorption isotherms on the model SWNT bundle at 77 K, The Feynman-Hibbs (FH) effective potential [20–26] were used to introduce quantum effects into intermolecular interactions. The FH effective potential can be successfully applied when systems are under usual densities and $\lambda_B^* \leq 0.5$, where $\lambda_B^* = \hbar/(mk_BT\sigma^2)^{1/2}$, m and σ are mass and size of a fluid molecule, and k_B is the Boltzmann constant, respectively [22,23]. The λ_B^*-value for H_2 at 77 K is 0.47, and thus the FH method should give identical results with those from the rigorous path integral method for quantum H_2 above 77 K.

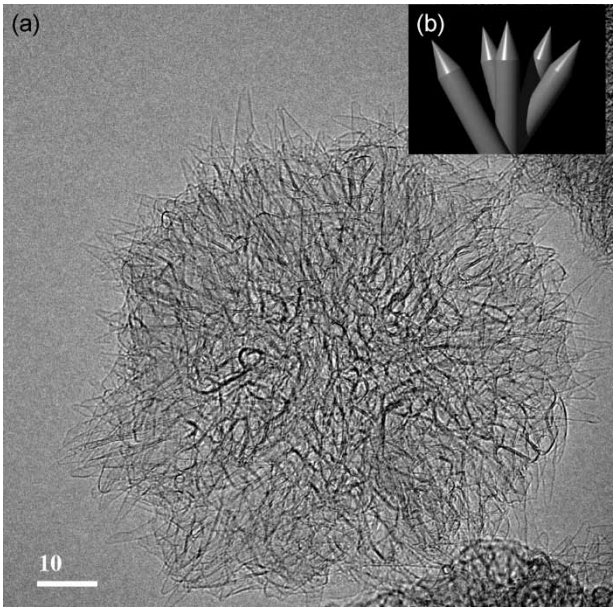

Figure 1. TEM image of the SWNH assembly (a) and a schematic representation of the SWNH particles (b).

2. Experimental

The as-grown SWNH sample was oxidized at 693 K to open nanoscale windows on the wall of the SWNH particle. Details of the oxidation method have been provided elsewhere [16]. The as-grown and oxidized SWNH samples are denoted by as-SWNH and ox-SWNH, respectively. The adsorption isotherms of H_2 at 20 K, H_2 and D_2 at 77 K, and N_2 at 77, 81, 85 and 92 K on the SWNH samples were measured with laboratory-designed volumetric adsorption equipment. The apparatus consists of a gas handling system and a cryostat with a He closed-cycle refrigerator. All samples were outgassed under a vacuum better than 0.1 mPa at 423 K for 2 h. The temperature was kept within ±0.05 K during adsorption measurements. Thermal transpiration was corrected by use of the empirical equation of Takaishi and Sensui [27].

3. Potential models and simulations

3.1 Fluid–fluid interaction potential

In this work, N_2, H_2, and D_2 molecules are treated as a structureless spherical particle, and thus we model the fluid–fluid interaction by the Lennard-Jones (LJ) potential

$$V_{LJ}(r) = 4\varepsilon_{ff}\left[\left(\frac{\sigma_{ff}}{r}\right)^{12} - \left(\frac{\sigma_{ff}}{r}\right)^{6}\right]. \quad (1)$$

The LJ interaction parameters used are, $\sigma_{ff} = 0.3615$ nm and $\varepsilon_{ff}/k = 101.5$ K for N_2, and $\sigma_{ff} = 0.2958$ nm and $\varepsilon_{ff}/k = 36.7$ K for H_2, respectively. Here, we used the FH effective potential for H_2 and D_2 adsorption at 77 K. In the FH treatment, a quantum fluid molecule is represented by a Gaussian wavepacket of width $\hbar/(12mk_BT)^{1/2}$; thus, the effective potential can be obtained by averaging the classical LJ potential over the Gaussian. If this Gaussian FH effective potential is

expanded to second order, the quadratic FH effective potential can be obtained

$$V_{\mathrm{FH}}(r) = V_{\mathrm{LJ}}(r) + \left(\frac{\hbar^2}{24\mu k_{\mathrm{B}}T}\right)\nabla^2 V_{\mathrm{LJ}}(r), \qquad (2)$$

where $\mu = m/2$ is the reduced mass of a pair of quantum molecules in interaction.

3.2 Fluid-SWNH interaction potential

We assumed here a homogeneous cylindrical tube like SWNT as a model of the SWNH particle, by ignoring the cone part of the SWNH particle. The fluid-SWNT interaction potential inside the tube can be modeled by the LJ potential integrated over an infinitely long tube, and that is given by [28,29]

$$V_{\mathrm{LJ}}^{\mathrm{internal}}(r,R) = \pi^2\rho_{\mathrm{s}}\varepsilon_{\mathrm{sf}}\sigma_{\mathrm{sf}}^2\left[\frac{63}{32}\frac{F(-4.5,-4.5,1.0;r^{*2})}{[R^*(1-r^{*2})]^{10}} - 3\frac{F(-1.5,-1.5,1.0;r^{*2})}{[R^*(1-r^{*2})]^4}\right], \qquad (3)$$

where r is the distance between a fluid molecule and the central axis of SWNT, $F(\alpha, \beta, \gamma; \chi)$ is a hypergeometric function, R is the radius of the tube, ρ_{s} is the density of solid atoms in the tube wall (in case of SWNT, $\rho_{\mathrm{s}} = 38.2\,\mathrm{nm}^{-2}$), $r^* = r/R$, and $R^* = R/\sigma_{\mathrm{sf}}$, respectively. For N_2-SWNT and H_2-SWNT interaction parameters, the combining rules of the form $\varepsilon_{\mathrm{sf}} = (\varepsilon_{\mathrm{ff}}\varepsilon_{\mathrm{ss}})^{1/2}$, $\sigma_{\mathrm{sf}} = (\sigma_{\mathrm{ff}} + \sigma_{\mathrm{ss}})/2$ were used with $\varepsilon_{\mathrm{ss}}/k_{\mathrm{B}} = 28\,\mathrm{K}$ and $\sigma_{\mathrm{ss}} = 0.34\,\mathrm{nm}$ (LJ parameters for graphite). Likewise, the fluid-SWNT interaction potential on the external surface of SWNT can be calculated as

$$V_{\mathrm{LJ}}^{\mathrm{external}}(r,R) = \pi^2\rho_{\mathrm{s}}\varepsilon_{\mathrm{sf}}\sigma_{\mathrm{sf}}^2\left[\frac{63}{32}\frac{r^{*11}F(-4.5,-4.5,1.0;r^{*2})}{[R^*(1-r^{*2})]^{10}} - 3\frac{r^{*5}F(-1.5,-1.5,1.0;r^{*2})}{[R^*(1-r^{*2})]^4}\right], \qquad (4)$$

where $r^* = R/r$.

Quantum H_2-SWNT interaction potentials for the internal and external of SWNT, which employs the pairwise FH effective potential (Eq. 2), can be also obtained by the similar way [30],

$$V_{\mathrm{FH}}^{\mathrm{internal}}(r,R) = V_{\mathrm{LJ}}^{\mathrm{internal}}(r,R) + \pi^2\rho_{\mathrm{s}}\varepsilon_{\mathrm{sf}}\left(\frac{\hbar^2}{mk_{\mathrm{B}}T}\right) \times \left[\frac{2541}{256}\frac{F(-5.5,-5.5,1.0;r^{*2})}{[R^*(1-r^{*2})]^{12}} - \frac{25}{8}\frac{F(-2.5,-2.5,1.0;r^{*2})}{[R^*(1-r^{*2})]^6}\right], \qquad (5)$$

and then

$$V_{\mathrm{FH}}^{\mathrm{external}}(r,R) = V_{\mathrm{LJ}}^{\mathrm{external}}(r,R) + \pi^2\rho_{\mathrm{s}}\varepsilon_{\mathrm{sf}}\left(\frac{\hbar^2}{mk_{\mathrm{B}}T}\right) \times \left[\frac{2541}{256}\frac{r^{*13}F(-5.5,-5.5,1.0;r^{*2})}{[R^*(1-r^{*2})]^{12}} - \frac{25}{8}\frac{r^{*7}F(-2.5,-2.5,1.0;r^{*2})}{[R^*(1-r^{*2})]^6}\right], \qquad (6)$$

where we used $\mu = m$ for the quantum H_2-carbon atom interaction differently from $\mu = m/2$ for the H_2—H_2 interaction, since we assumed that the carbon atoms are rigidly linked together inside the SWNT wall.

An isolated SWNT model was used to model the endohedral adsorption on the SWNH particle, as noted above. The diameter of the SWNT model was set to 3.2 nm, according to Ohba *et al.* [15]. Then, from TEM observations, it is clear that the SWNH assembly has at least two adsorption sites: an interstitial channel (the space between the tubular parts of the SWNH particles; abbreviated IC) and an external surface of the SWNH particle, which protrudes from the SWNH assembly (see figure 1). Thus, in this study, we assumed that the structure of the SWNH assembly could be modeled by a SWNT bundle with a finite number of tubes. The model of the SWNT bundle is shown in figure 2. The SWNT bundle model consists of a hexagonal bundle containing seven SWNTs with a tube diameter, $D = 3.2\,\mathrm{nm}$, and a van der Waals gap between tubes, $g = 0.4\,\mathrm{nm}$. In the SWNT bundle model, SWNTs are close-ended tube, and thus there are three adsorption sites for adsorbates: IC between three SWNTs, a groove site between two outer tubes of the bundle, and an outer surface of a tube on the surface of the bundle, respectively.

4. Isosteric heat of adsorption

We calculated the isosteric heat of adsorption to evaluate the N_2-SWNT interaction potential. The isosteric heat of

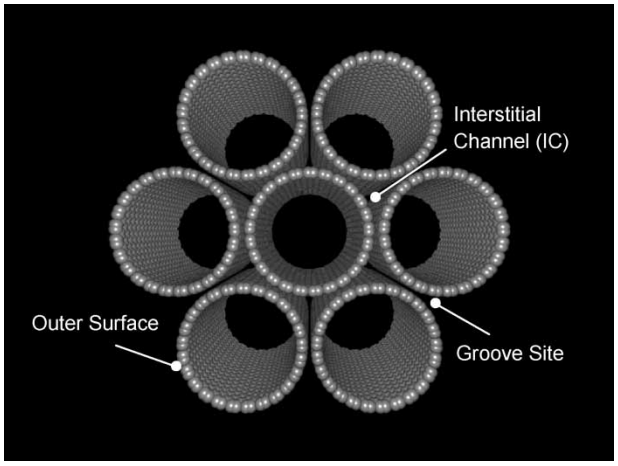

Figure 2. Schematic representation of the SWNT bundle model.

adsorption can be computed from the fluctuations in the number of adsorbed molecules and the potential energy

$$q_{st} = k_B T - \frac{\langle UN\rangle - \langle U\rangle\langle N\rangle}{\langle N^2\rangle - \langle N\rangle^2}, \quad (7)$$

where q_{st} is the isosteric heat of adsorption, N is the number of adsorbates, and U is the total energy, respectively.

5. Simulation details

The GCMC method based on the classical LJ potential was used to simulate classical N_2 adsorption at 77 K, and H_2 at 20 K. The probabilities to attempt a single displacement, creation, and deletion were set to 0.4, 0.3, and 0.3, respectively. The system was equilibrated for 1×10^7 Monte Carlo (MC) steps, after which data were corrected for 1×10^7 steps. The fluid–fluid interaction was truncated at distance of 5 σ_{ff}. Periodic boundary conditions were applied along the tube axis for the endohedral adsorption on the isolated SWNT model, and all three directions for the adsorption on the SWNH bundle model, respectively. The tube length of 10 σ_{ff} was used for the both models. In the grand canonical ensemble, the volume, temperature, and chemical potential are fixed; however, to compare with experimental isotherms as a function of a bulk fluid pressure, it is needed to obtain the pressure of the bulk fluid as a function of the chemical potential and temperature. We have therefore performed canonical MC simulation with the LJ and FH effective potentials, which is combined with the Widom test particle insertion method [31], to determine the excess chemical potential. The pressures of the classical and quantum fluids were simultaneously calculated during the MC simulations.

6. Results and discussion

Figures 3 and 4 show adsorption isotherms of N_2 at 77 K and H_2 at 20 K on as-SWNH and ox-SWNH, respectively. Here, the adsorption isotherms of H_2 and N_2 in the internal space of SWNHs were calculated by subtracting the adsorption isotherm on as-SWNH from that on ox-SWNH, and are also shown in figures 3 and 4. From the preceding TEM observation, it has been confirmed that the assembly structure of ox-SWNH sample does not change on the oxidation process. Therefore, the adsorption isotherms obtained by the subtraction can be regard as those only in the internal tube nanospaces.

6.1 N_2 adsorption on the SWNH assembly at 77 K

The adsorption isotherm for N_2 on the SWNT bundle from the GCMC simulations are shown in figure 5a and b. The simulated adsorption amount (mmol/g) for the SWNT bundle model was divided by the BET surface area (983 m^2/g) obtained from the simulated isotherm itself, and then the values was multiplied by the experimental BET surface area (358 m^2/g) for as-SWNH to compare with the experimental adsorption isotherm on as-SWNH. Figure 6a–d show the snapshots from the GCMC simulations. The simulations show that N_2 molecules adsorb in ICs of the SWNT bundle around $P/P_0 = 10^{-7}$ (figure 6a), and one-dimensional phases of N_2 are formed on the groove sites at about $P/P_0 = 10^{-5}$ (figure 6b). The experimental isotherm on as-SWNH shows a significant adsorption at $P/P_0 = 10^{-5}$, and thus this suggests that the SWNH assembly has adsorption sites with strong interaction potentials between SWNHs at least like the groove site of the SWNT bundle model. The simulations predict the monolayer completion on the outer surface of the SWNT bundle around $P/P_0 = 0.01$ (figure 6d), and are in good agreement with the experimental adsorption isotherm on as-SWNH over a wide range of relative pressures above $P/P_0 = 0.01$ (figure 5). This indicates that after the monolayer completion, the adsorption process of N_2 on the outer surface of SWNT is similar to that on the external surface of SWNH. In the SWNT bundle model, the second layer of adsorbed N_2 is not completed near saturated vapor pressure, that is, the multilayer adsorption on the external surface of the tube-like wall (including SWNH) is hard to be achieved because of the relatively weak solid-fluid interactions. Then, the steep rise in adsorption on the SWNH assembly over $P/P_0 = 0.8$ would be attributed to a capillary condensation between the SWNH assemblies. Note that the adsorption step for the bundle model around $P/P_0 = 0.01$ is more distinct compared with that for the experimental isotherm on as-SWNH. This is because the ratio of the outer surface area of the SWNT bundle to its ICs is larger than that for the SWNH assembly.

The isosteric heats of adsorption, q_{st}, from the simulations are shown in figure 7 together with the experimental data for the SWNH assembly which were calculated from the adsorption isotherms at 77–92 K. We found four characteristic peaks in the q_{st} curve from the simulations, which correspond to (1) filling of N_2 molecules in IC, (2) formation of a 1D phase of N_2 on the groove site, (3) formation of a 2-strip phase of N_2 over the 1D phase of N_2 on the groove site, (4) monolayer completion of N_2 on the outer surface of SWNT, respectively. Before the monolayer completion, the q_{st}-values from the experiments are high compared with those from the simulations. This should be attributed to incomplete arrangement of the SWNH particles in their assembly. In contrast, the monolayer heats from the simulations are in good agreement with the experimental data. This suggests that the assumed N_2-SWNT potential is relatively accurate and that only adsorption on the heterogeneous ICs in the SWNH assembly gives the discrepancy between the simulations and experiments.

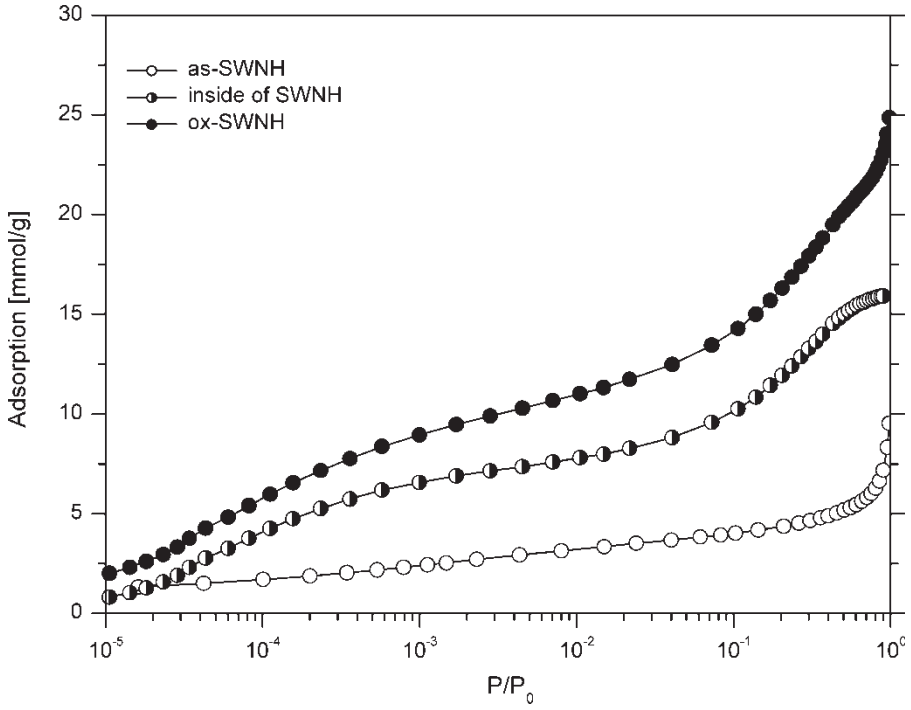

Figure 3. N_2 adsorption isotherms on as-SWNH, ox-SWNH, and the internal space of SWNHs at 77 K.

6.2 N_2 adsorption inside SWNH at 77 K

The simulated endohedral adsorption isotherm on the isolated SWNT models is presented in figure 8, together with the experimental isotherm on the internal space of the SWNH particle. The adsorption (mmol/g) experimentally obtained for the inside of SWNHs was divided by the pore volume (0.55 cm^3/g) calculated by using the bulk liquid density (28.9 mmol/cm^3), to make a comparison between the simulated and experimental adsorption isotherms. The simulated adsorption isotherm has a step-like behavior at $P/P_0 = 10^{-4}$, indicating the monolayer completion on the internal wall of the SWNT model. However the experimental isotherm inside SWNHs exhibits a gradual

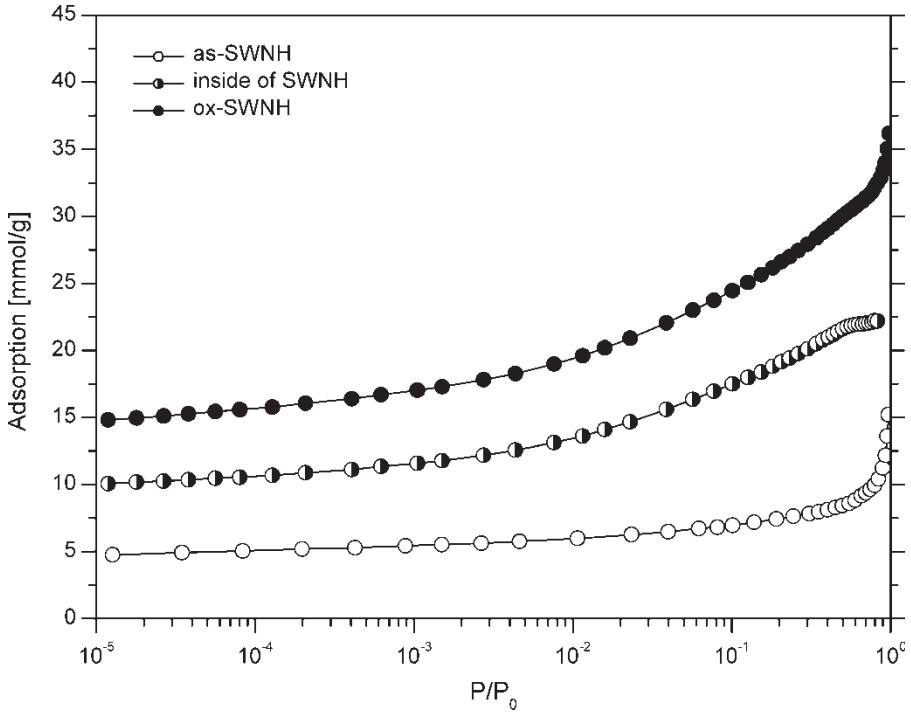

Figure 4. H_2 adsorption isotherms on as-SWNH, ox-SWNH, and the internal space of SWNHs at 20 K.

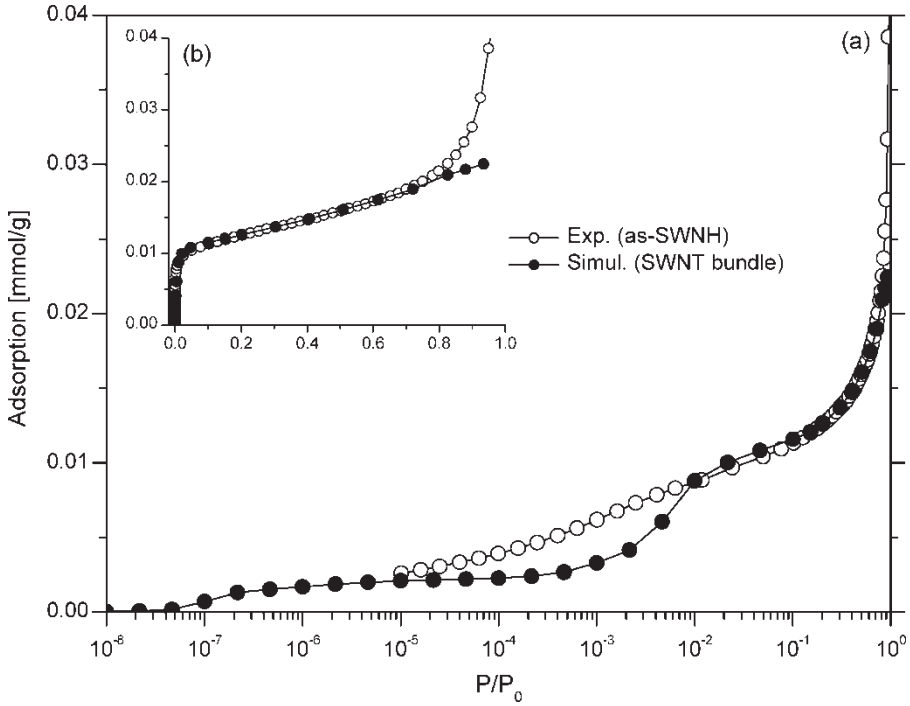

Figure 5. Comparison between the experimental N_2 adsorption isotherm on as-SWNH and simulated isotherm for the SWNT bundle model at 77 K. The pressures are given in (a) logarithmic and (b) linear scales.

step from lower P/P_0 than the SWNT model. This should be mainly attributed to the filling in the tubular part of the SWNH particle less than 3 nm in diameter, including the cone part. Two first order transitions in the simulated isotherm at $P/P_0 \sim 0.1$ correspond to spontaneous capillary condensation and evaporation transitions (vapor-like and liquid-like spinodals), and thus an equilibrium transition should exist within the hysteresis loop between the spinodals. However, the experimental data show a gradual increase over $P/P_0 \sim 0.1$, corresponding to the capillary condensation inside SWNHs. This suggests that SWNHs have relatively wide tube size distributions, and this has already reported in the previous study [18].

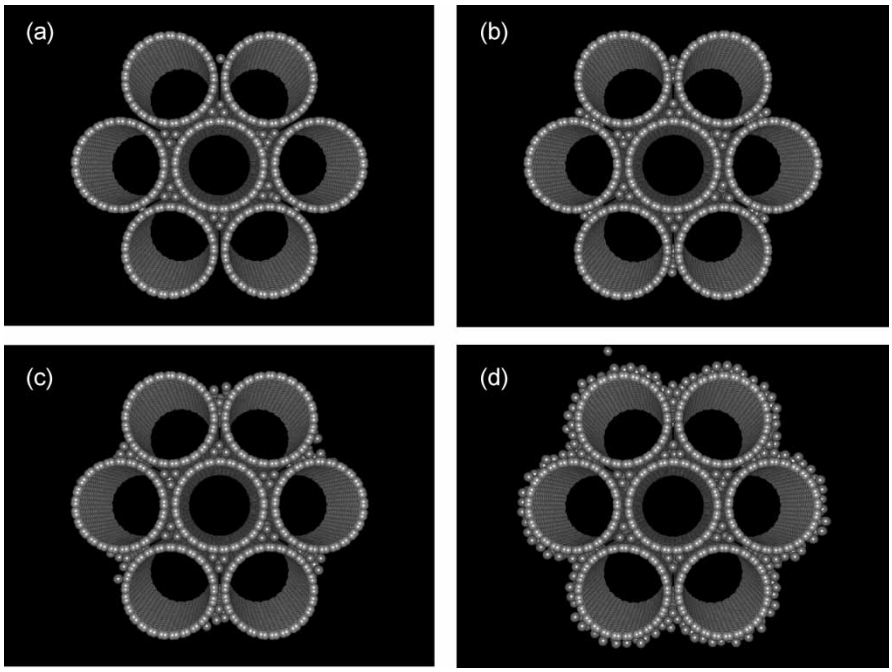

Figure 6. Snapshots of adsorbed N_2 molecules on the SWNT bundle from the GCMC simulations at (a) $P/P_0 = 2 \times 10^{-7}$, (b) $P/P_0 = 10^{-5}$, (c) $P/P_0 = 10^{-3}$, and (d) $P/P_0 = 10^{-2}$, respectively. The blue and gray spheres represent N_2 molecules and carbon atoms of SWNT, respectively.

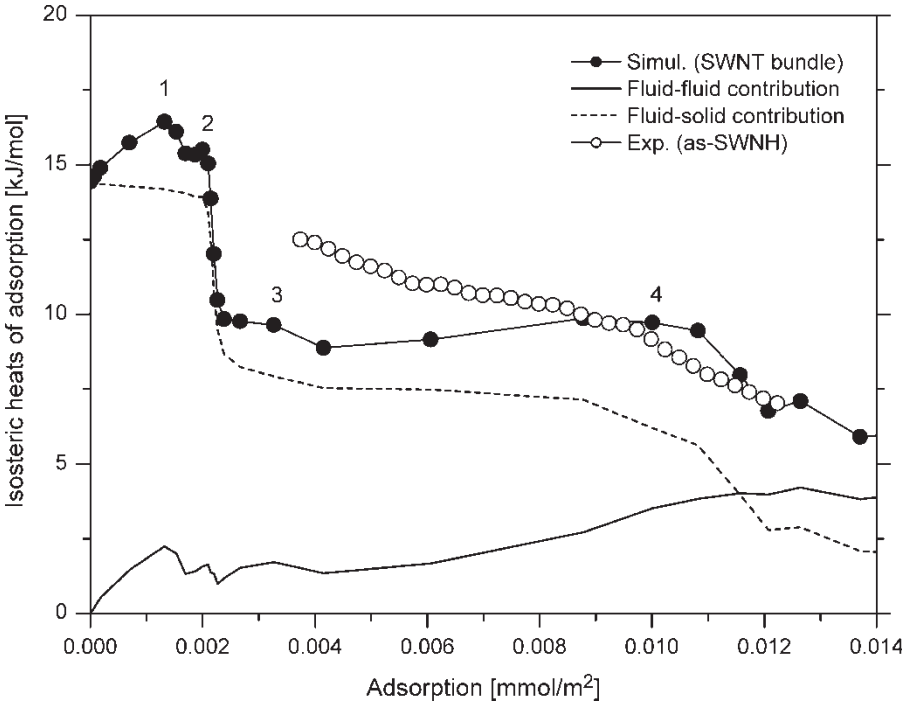

Figure 7. Comparison between isosteric heats of adsorption of N_2 from the experiments for as-SWNH and simulations for the SWNT bundle model.

6.3 H_2 adsorption inside SWNH at 20 K

Figure 9 shows the simulated adsorption isotherm of classical H_2 inside the isolated SWNT model and the experimental H_2 isotherm in the interior of SWNHs at 20 K. The adsorption amount of H_2 (mmol/g) from the experiments were divided by the pore volume of the inside of SWNHs (0.55 cm^3/g) obtained from the experimental N_2 isotherm to roughly estimate a volumetric density of adsorbed H_2, and make a comparison with the results from the GCMC simulations. The simulated adsorption isotherm gives a steep completion of the monolayer on the internal wall of SWNT at 10^{-11} MPa, and a discontinuous second layer formation at 10^{-5} MPa,

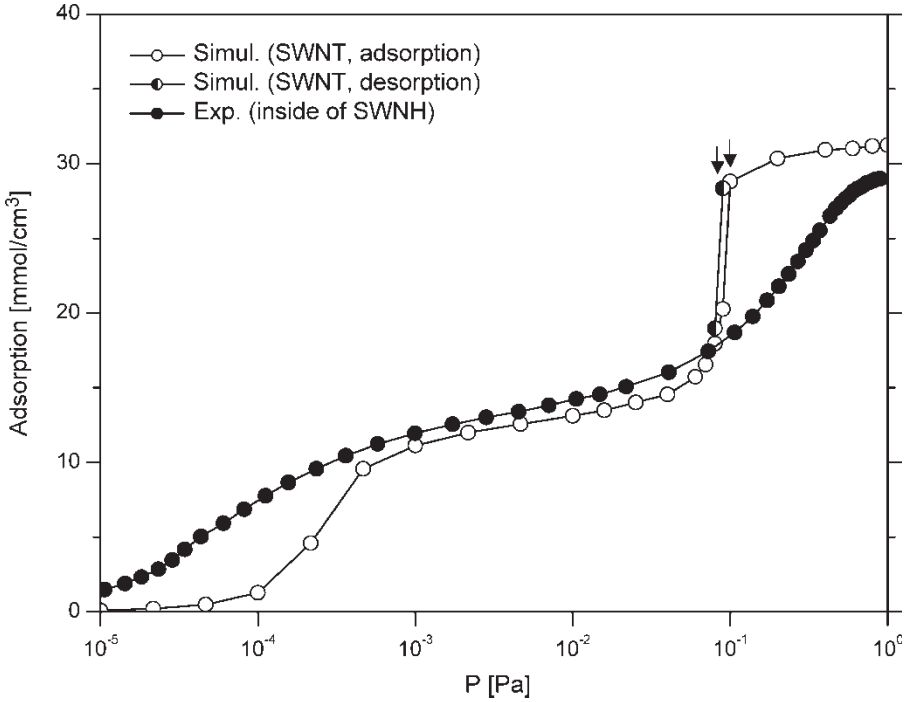

Figure 8. Adsorption isotherms of N_2 inside the SWNT model by the GCMC simulations and the experimental isotherm in the interior of SWNHs at 77 K. The arrows denote the positions of the spontaneous capillary condensation (right) and desorption (left), respectively.

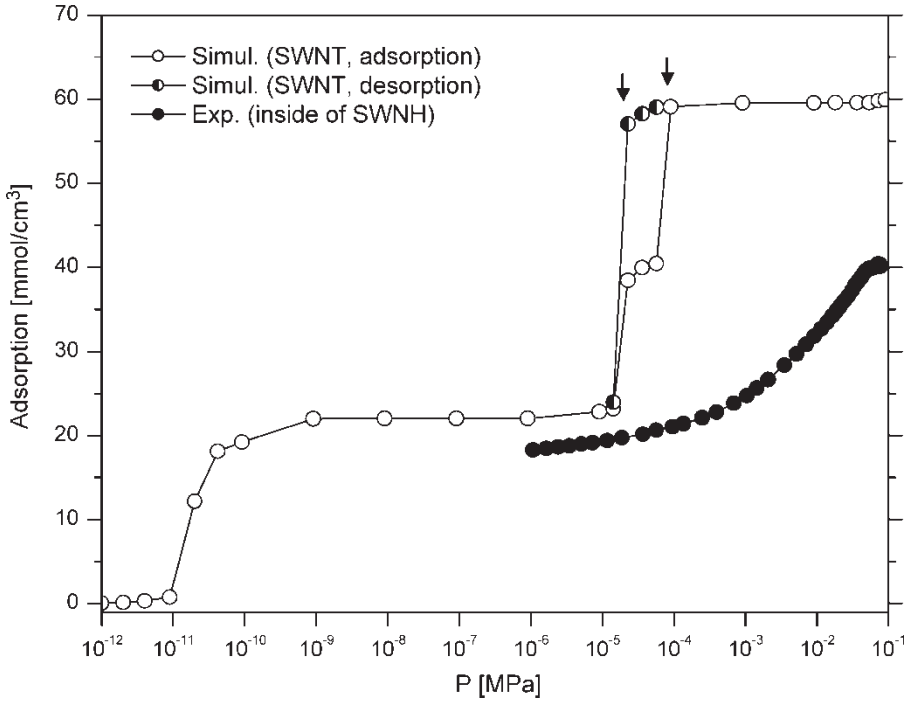

Figure 9. Adsorption isotherms of H_2 inside the SWNT model by the GCMC simulations with the classical LJ system and the experimental H_2 isotherm in the interior of SWNHs at 20 K. The arrows denote the positions of the spontaneous capillary condensation (right) and desorption (left), respectively.

which are an indication of the first order transitions. The adsorption isotherm of classical H_2 also exhibits another two first order transitions corresponding to the spontaneous capillary condensation and desorption in the center of the SWNT model. Therefore, the equilibrium desorption should occur at between the two transitions. The volumetric densities of classical H_2 from the GCMC simulations are substantially higher than the experimental data. The difference can be explained in terms of the effective radius of quantum H_2 being larger than that of classical H_2, and thus this indicates that quantum effects are very important at 20 K, and the classical H_2 adsorption is not even qualitatively correct.

6.4 H_2 adsorption on the SWNT assembly and the GCMC simulations based on the FH effective potential

We have performed GCMC simulations based on the FH effective potential (FH-GCMC) for H_2 and D_2 adsorption on the SWNT bundle model at 77 K. The simulated adsorption isotherms are shown in figure 10, together with the experimental isotherms of the hydrogen isotopes on the SWNH assembly at 77 K. The experimental data represent a gradual uptake of the hydrogen isotopes from 10^{-5} MPa; however, the predictions from the FH-GCMC simulations show that the adsorption of the hydrogen isotopes in ICs of the SWNT bundle start from about 10^{-4} MPa. This indicates that the SWNH assembly has narrower ICs than those of the SWNT bundle model, and the narrow ICs may exist around the core of the SWNH assembly. Although it is difficult to qualitatively compare the FH-GCMC simulations and the experimental data with respect to quantum effects as mentioned above, we have calculated the ratio of H_2 adsorption to D_2 from the simulations and experiment as a function of pressure (figure 11a and b). The H_2/D_2 ratio from the FH-GCMC simulations is 0.835 ± 0.01 over the range of pressures from 10^{-5} to 10^{-3} MPa, and increase to about 0.91 at 0.1 MPa. Below 10^{-3} MPa, most hydrogen isotopes are preferentially adsorbed only in ICs of the SWNT bundle model. Therefore, the large difference in adsorption between H_2 and D_2 at low pressure should be attributed to significant quantum effects, that is, the potential field of IC for H_2 is weak because of the wide quantum spreading of a H_2 molecule (proportional to $\hbar/(6mk_BT)^{1/2}$) compared with D_2. Note that the difference in adsorption between quantum and classical H_2 should be larger than that between quantum H_2 and D_2 at 77 K. The H_2/D_2 ratios from the experiments are always smaller than the FH-GCMC simulations over the whole range of pressures. This may be attributed to the narrow ICs of the SWNH assembly because the H_2/D_2 ratio should be large in a pore, which has a width comparable to the diameter of molecular quantum H_2 at 77 K.

7. Conclusion

We have compared the experimental adsorption isotherm of N_2 on as-SWNH at 77 K with the GCMC isotherm for the SWNT bundle model. The simulated N_2 adsorption isotherm is in reasonably good agreement with the experimental results after the monolayer completion on

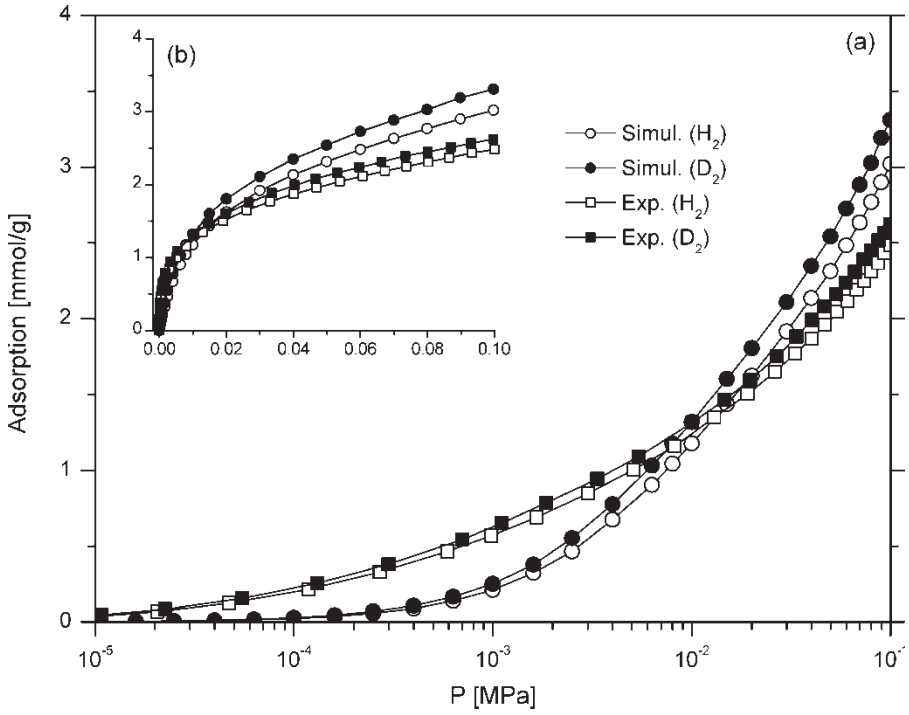

Figure 10. Adsorption isotherms of H_2 and D_2 from the FH-GCMC simulations for the SWNT bundle model and experiment for as-SWNH at 77 K. The pressures are given in (a) logarithmic and (b) linear scales.

the outer surface of the SWNT bundle, and this has been also confirmed from the isosteric heats of adsorption. The discrepancy between the experimental and simulation isotherms below the monolayer completion suggests that SWNHs are heterogeneously arranged in the SWNH assembly.

We have compared the experimental H_2 isotherm inside SWNHs with simulated one of classical H_2 in the internal space of the isolated SWNT model at 20 K. It shows that the density of adsorbed H_2 inside SWNHs is quite smaller than that of classical H_2 in the SWNT model due to large quantum effects. The FH-GCMC simulations for

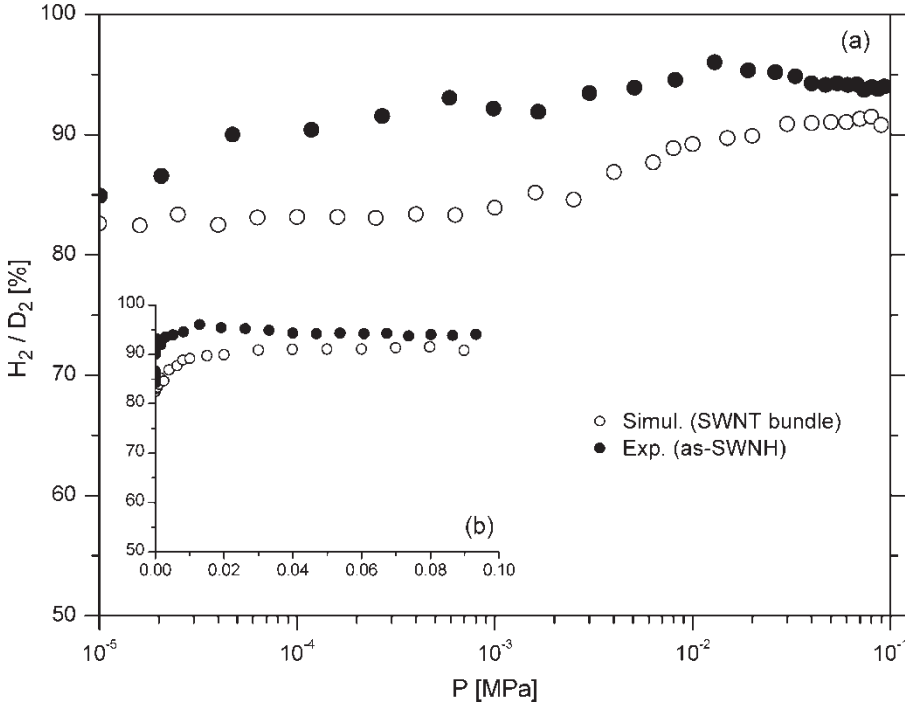

Figure 11. Ratio of H_2 adsorption to D_2 from the FH-GCMC simulations for the SWNT bundle model and experiments for as- SWNH as a function of pressure at 77 K. The pressures are given in (a) linear and (b) logarithmic scales.

hydrogen isotopes adsorption on the SWNT bundle at 77 K suggest that the SWNH assembly has narrower ICs than those of the SWNT bundle model. The difference in adsorption between H_2 and D_2 from the FH-GCMC simulations is large at low pressure; this is because the potential field of IC of the SWNT bundle for H_2 is relatively weaker than that for D_2 even at 77 K, due to the wide quantum spreading of a H_2 molecule.

Acknowledgements

This work was supported by the NEDO project on evaluation of hydrogen storage on nanocarbon.

References

[1] S. Iijima, T. Ichihashi. Single-shell carbon nanotubes of 1-nm diameter. *Nature*, **363**, 603 (1993).
[2] D.S. Bethune, C.H. Kiang, M.S. de Vries, G. Gorman, R. Savoy, J. Vazquez, R. Beyers. Cobalt-catalyzed growth of carbon nanotubes with single-atomic-layer walls. *Nature*, **363**, 605 (1993).
[3] A.C. Dillon, K.M. Jones, T.A. Bekkedahl, C.H. Kiang, D.S. Bethune, M.J. Heben. Storage of hydrogen in single-walled carbon nanotubes. *Nature*, **386**, 377 (1997).
[4] C. Liu, Y.Y. Fan, M. Liu, H.T. Cong, H.M. Cheng, M.S. Dresselhaus. Hydrogen storage in single-walled carbon nanotubes at room temperature. *Science*, **286**, 1127 (1999).
[5] M. Rzepka, P. Lamp, M.A. de la Casa-Lillo. Physisorption of hydrogen on microporous carbon and carbon nanotubes. *J. Phys. Chem. B*, **102**, 10894 (1998).
[6] Y.F. Yin, T. Mays, B. McEnaney. Molecular simulations of hydrogen storage in carbon nanotube arrays. *Langmuir*, **16**, 10521 (2000).
[7] K.A. Williams, P.C. Eklund. Monte Carlo simulations of H_2 physisorption in finite-diameter carbon nanotube ropes. *Chem. Phys. Lett.*, **320**, 352 (2000).
[8] Q. Wang, J.K. Johnson. Molecular simulation of hydrogen adsorption in single-walled carbon nanotubes and idealized carbon slit pores. *J. Chem. Phys.*, **110**, 577 (1999).
[9] N. Setoyama, K. Kaneko. Density of He adsorbed in micropores at 4.2 K. *Adsorption*, **1**, 165 (1995).
[10] D. Nemirovsky, R. Moreh, K.H. Andersen, J. Mayers. Anomalous kinetic energies of adsorbed ^{4}He on active carbon fiber (ACF). *J. Phys. Cond. Matter*, **11**, 6653 (1999).
[11] D. Nemirovsky, R. Moreh, K. Kaneko, T. Ohba, J. Mayers. Kinetic energy of neon atoms adsorbed on activated carbon. *Surf. Sci.*, **526**, 282 (2003).
[12] H. Tanaka, M. El-Merraoui, T. Kodaira, K. Kaneko. Possibility of quantum effect in micropore filling of Ne on $AlPO_4$-5. *Chem. Phys. Lett.*, **351**, 417 (2002).
[13] S. Iijima, M. Yudasaka, R. Yamada, S. Bandow, K. Suenaga, F. Kokai, K. Takahashi. Nano-aggregates of single-walled graphitic carbon nano-horns. *Chem. Phys. Lett.*, **309**, 165 (1999).
[14] K. Murata, K. Kaneko, W.A. Steele, F. Kokai, K. Takahashi, D. Kasuya, M. Yudasaka, S. Iijima. Porosity evaluation of intrinsic intraparticle nanopores of single wall carbon nanohorn. *Nano Lett.*, **4**, 197 (2001).
[15] T. Ohba, K. Murata, K. Kaneko, W.A. Steele, F. Kokai, K. Takahashi, D. Kasuya, M. Yudasaka, S. Iijima. N_2 adsorption in an internal nanopore space of single-walled carbon nanohorn: GCMC simulation and experiment. *Nano. Lett.*, **7**, 371 (2001).
[16] K. Murata, K. Kaneko, W.A. Steele, F. Kokai, K. Takahashi, D. Kasuya, K. Hirahara, M. Yudasaka, S. Iijima. Molecular potential structures of heat-treated single-wall carbon nanohorn assemblies. *J. Phys. Chem. B*, **105**, 10210 (2001).
[17] E. Bekyarova, K. Murata, M. Yudasaka, D. Kasuya, S. Iijima, H. Tanaka, H. Kanoh, K. Kaneko. Single-wall nanostructured carbon for methane storage. *J. Phys. Chem. B*, **107**, 4681 (2003).
[18] H. Tanaka, M. El-Merraoui, H. Kanoh, W.A. Steele, M. Yudasaka, S. Iijima, K. Kaneko. Quantum effects on hydrogen adsorption in internal nanospaces of single-wall carbon nanohorns. *J. Phys. Chem. B*, **108**, 17457 (2004).
[19] M.P. Allen, D.J. Tildesley. *Computer Simulation of Liquids*, Clarendon Press, Oxford (1987).
[20] R.P. Feynman, A. Hibbs. *Quantum Mechanics and Path-Integrals*, McGraw-Hill, New York (1965).
[21] R.P. Feynman. *Statistical Mechanics*, Benjamin, New York (1972).
[22] L.M. Sesé. Study of the Feynman-Hibbs effective potential against the path-integral formalism for Monte Carlo simulations of quantum many-body Lennard-Jones systems. *Mol. Phys.*, **81**, 1297 (1994).
[23] L.M. Sesé. Feynman-Hibbs potentials and path integrals for quantum Lennard-Jones systems: theory and Monte-Carlo simulations. *Mol. Phys.*, **85**, 931 (1995).
[24] F. Darkrim, D.J. Levesque. Monte Carlo simulations of hydrogen adsorption in single-walled carbon nanotubes. *J. Chem. Phys.*, **109**, 4981 (1998).
[25] F. Darkrim, A. Aoufi, D. Levesque. Quantum contribution to gas adsorption in carbon nanotubes. *Mol. Simul.*, **24**, 51 (2000).
[26] F. Darkrim, D. Levesque. High adsorptive property of opened carbon nanotubes at 77 K. *J. Phys. Chem. B*, **104**, 6773 (2000).
[27] T. Takaishi, Y. Sensui. Thermal transpiration effect of hydrogen, rare gases, and methane. *Trans. Farad. Soc.*, **53**, 2503 (1963).
[28] G.J. Tjatjouls, D.L. Feke, J.A. Mann Jr. Molecule-micropore interaction potentials. *J. Phys. Chem.*, **92**, 4006 (1988).
[29] H. Tanaka, M. El-Merraoui, W.A. Steele, K. Kaneko. Methane adsorption on single-walled carbon nanotube–a density functional theory model. *Chem. Phys. Lett.*, **352**, 334 (2002).
[30] H. Tanaka, J. Fan, H. Kanoh, M. Yudasaka, S. Iijima, K. Kaneko, Quantum effects on hydrogen isotope adsorption on single-wall carbon nanohorns. submitted for publication in *J. Am. Chem. Soc*
[31] B. Widom. Some topics in the theory of fluids. *J. Chem. Phys.*, **39**, 2802 (1963).